J Bionic Eng 17 (2020) 600–610
DOI: https://doi.org/10.1007/s42235-020-0048-x

Journal of Bionic Engineering
http://www.springer.com/journal/42235

How do Cats Resist Landing Injury: Insights into the Multi-level Buffering Mechanism

Xueqing Wu[1,2], Baoqing Pei[1,2*], Yuyang Pei[3], Wei Wang[1,2], Yan Hao[1,2], Kaiyuan Zhou[1,2]

1. *School of Biological Science and Medical Engineering*, *Beihang University*, *Beijing* 100083, *China*
2. *Beijing Advanced Innovation Centre for Biomedical Engineering*, *Beihang University*, *Beijing* 100083, *China*
3. *School of Public Health*, *Nanjing Medical University*, *Nanjing* 211166, *China*

Abstract

When humans jump down from a high position, there is a risk of serious injury to the lower limbs. However, cats can jump down from the same heights without any injury because of their excellent ability to attenuate impact forces. The present study aims to investigate the macro/micro biomechanical features of paw pads and limb bones of cats, and the coordination control of joints during landing, providing insights into how cats protect themselves from landing injury. Accordingly, histological analysis, radiological analysis, finite element method, and mechanical testing were performed to investigate the mechanical properties, microstructure, and biomechanical response of the pads and limb bones. In addition, using a motion capture system, the kinematic/kinetic data during landing were analysed based on inverse dynamics. The results show that the pads and limb bones are major contributors to non-impact-injuries, and cats actively couple their joints to adjust the parameters of movement to dissipate the higher impact. Therefore, the paw pads, limb bones, and coordinated joints complement each other and constitute a multi-level buffering mechanism, providing the cat with the sophisticated shock absorption system. This biomechanical analysis can accordingly provide biological inspiration for new approaches to prevent human lower limb injuries.

Keywords: cat, multi-level buffering, paw pads, limb bones, coordinated joints

1 Introduction

Cats can jump down from a high position without any injury because of their superior landing buffering capacities which they have achieved through natural selection. This phenomenon has drawn widespread attention. Numerous cases of feline high-rise syndrome have shown that the survival rate of cats is as high as 96.5% after the fall[1]. The saying that cats have nine lives also reflects the fact that cats indeed have a remarkable ability to dissipate the impact of a fall, which is usually lethal for humans.

From the biomechanical viewpoint, the paw pads, limb bones, and coordinated joints can act as dampers for cats, forming a multi-level (foot-level, limb-level, and joint level) buffering process during landing to effectively dissipate the impact force. As paw pads are the only body parts that touch the ground during landing, paw pads of the foot-level should be studied first. The human plantar and infrapatellar fat pads are known to share a remarkable ability to distribute and damp mechanical stresses during locomotion[2,3]. Similarly, cat paw pads involve a cushioning role during landing, thus attenuating the ground impact and protecting internal structures[4]. Therefore, mechanical tests have been conducted, which show that paw pads have viscoelastic properties in which damping helps absorb the impact energy and prevent loss of contact with the ground[5]. Meanwhile, the importance of viscoelastic properties of footpads has also been emphasised by studying its functional morphology and biomechanics. The results suggest that pads should have a certain amount of flexibility, stiffness, and damping to maintain stability and dissipate and transfer impact force[6].

Second, native bones are nanocomposites, primarily composed of cells, fibrous protein, collagen, hydroxyapatite, and water, and they exhibit high strength in self-assembly and nanofabrication[7,8]. There is also overwhelming evidence that the mechanical behaviour

***Corresponding author:** Baoqing Pei
E-mail: pbq@buaa.edu.cn

and strength of bones can adapt to environmental changes because their mineral masses and microstructure are susceptible to mechanical loading[9]. For example, in outer space, the reduction of mechanical load can lead to bone loss, similar to osteoporosis, thus reducing bone strength[10,11]. Nowadays, CT can help perform accurate and non-invasive analysis of bone microstructure in correlation with mechanical properties[12,13]. A study using radiographs of the sabretooth cat indicated that its enhanced forelimb strength, attributed to the thickening cortical bone, is part of an adaptive product of the need for hunting[14]. Thus, a logical explanation to resist landing injury in view of bone biomaterials based on the limb-level is required.

Finally, the mechanical energy can be dissipated and transferred by manipulating the joint kinematics, and joint muscles are the major sites for absorption of energy. Cat full-body mechanics and the activity of joint muscles have been studied previously, which have shown that the coordination control of limbs and muscle activity appear to contribute to maintain statical stability in the frontal plane during narrow-path walking[15]. Also based on the cat walking gait, a 3D multiplane hindlimb kinematic model has been developed for the first time, providing important benefits for more accurate analysis of cat movement[16]. Regarding cat jumping, cases of falling cats have shown that they can bend back using their spines so that their forelimbs and hindlimbs land in turn, regardless of the direction in which the cat starts falling[17]. In addition, some researchers have investigated the distribution of Vertical Ground Reaction Forces (VGRFs) in the fore and hind limbs of cats and have shown that it is related to the jump height. The hindlimbs have been found to play an increasing role in energy absorption with increasing jump height[18]. Furthermore, the activity of joint muscles, which is critical during landing, can be determined by the jumping conditions[19]. Therefore, it is necessary to investigate the coordination control of joints to better understand energy absorption at the joint level.

However, little attention has been paid to the multi-level buffering mechanism (Fig. 1 and Videos) during landing in cats. The objective of this work is therefore to investigate the role of macro/micro biomechanical features of paw pads and limb bones and the coordination control of joints in avoiding impact injury of cats. In this study, the mechanical properties, microstructure, and biomechanical response of the pads and bones were investigated using various methods such as histological analysis, radiological analysis, Finite Element Model (FEM), and mechanical testing. Furthermore, the kinematic/kinetic data of experiments in which cats self-initiated jumps from different heights were analysed based on inverse dynamics. The results of this study will help interpret and understand the impact resistance biomechanism in cats.

2 Materials and methods

2.1 Ethical statement

All animal experiments were ethically reviewed by the Science and Ethics Committee of School of Biological Science and Medical Engineering of Beihang University.

2.2 Paw pad biomechanics

To investigate the microstructure of the paw pads, first, the larger metacarpal pads were selected, sectioned, and stained for histological examination. However, the spatial arrangement of the 3D compartments was still not clear. Then, we performed micro-CT scanning (Skyscan1272, Skyscan, Belgium), and the Dicom images were reconstructed using Mimics 17.0.

Based on the microstructure obtained from the above methods, a FEM composed of the epidermis layer, dermis layer, collagenous membranes, and ellipsoidal adipose chambers was established to simulate the overall biomechanical response of the pad under a compressive load. Notably, we also built a FEM with cylindrical adipose chambers for comparison. Because of the irregular distribution of adipose compartments, we simplified the adipose chambers to a micro-model comprising two layers, shifted from each other according to a hexagonal scheme, which has been proved to be an appropriate interpretation for the actual conformation of the subcutaneous tissue[2]. In addition, the material properties of the four parts were set according to previous studies[20,21]. The top sides of the two models were applied to a downward load of up to approximately 10 N. The bottom sides were fixed, whereas the lateral sides were unconstrained. Finally, the

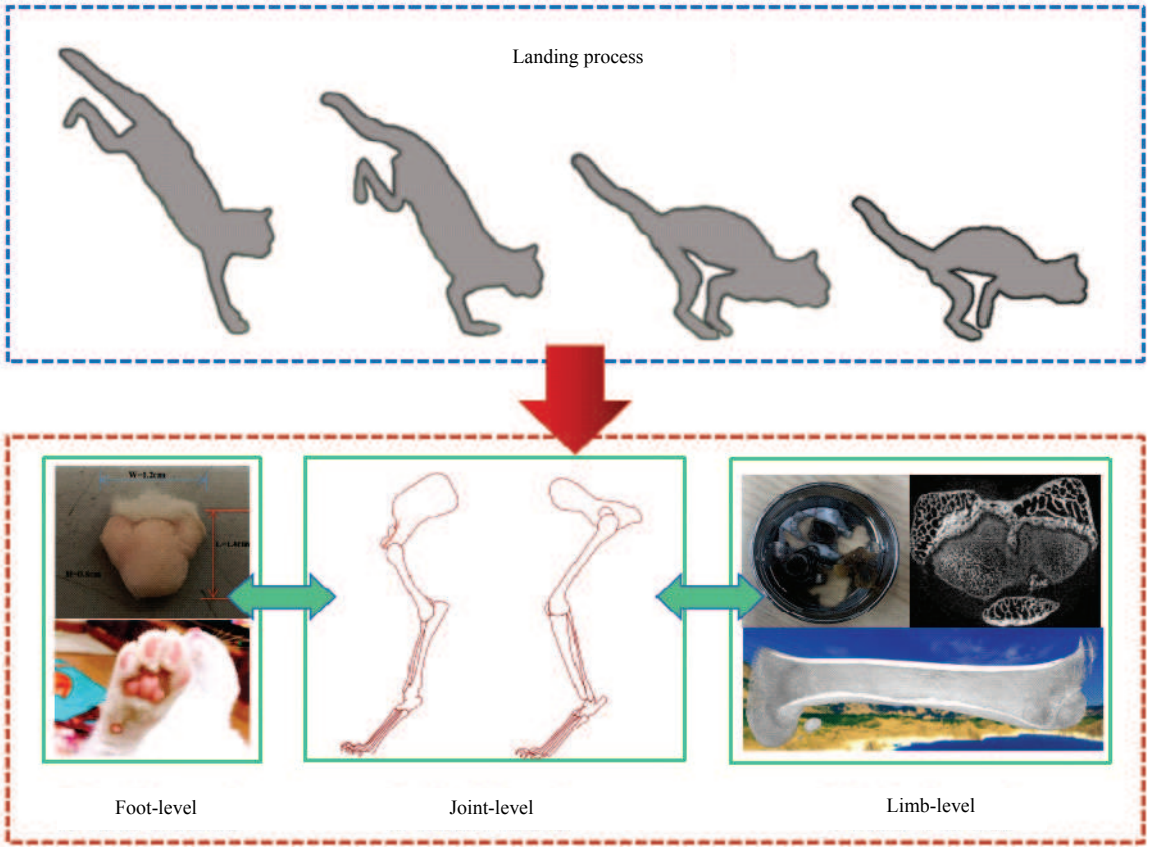

Fig. 1 Schematic depiction of the multi-level buffering mechanism.

contours of Von Mises and displacements were recorded and analysed.

2.3 Bone biomaterials

The humeri, ulnas, radiuses, femurs, tibias, and fibulas of the cats were all excised, bandaged with gauzes soaked in saline, and preserved at −20 ˚C. The long bones of the right limbs were slowly thawed to room temperature, and half of the specimens were subjected to three-point bending tests using an Instron testing machine (Instron E10000, USA). For a given specimen, the span was approximately ten times the external diameter of the cross section in the middle of the bone shaft. Before the bending tests, a preloading force (10 N) of 5 cycles was applied to the medial surface at a rate of 0.1 $mm \cdot s^{-1}$, and then, the bending loads were applied at a rate of 0.2 $mm \cdot s^{-1}$ until the specimen fractured. After each test, both the external and internal diameters of the cross section at the site of fracture were measured, and the maximum load, breaking load, stiffness, and elastic modulus of the bone midshaft were analysed. Briefly, the maximum load and breaking load were determined as the highest point and failure point of the load-deformation curve, respectively, and the stiffness was defined as the tangent modulus of the linear part of the curve. The elastic modulus was calculated considering the specimen as a hollow elliptical tube[22].

Half of the remaining specimens were subjected to a micro-CT scan (SkyScan 1076, Belgium). The region of interest commenced at the position near the growth plate level and extended to the diaphysis at 3.5 mm. Morphometric variables of trabeculae, including bone volume fraction (BV/TV), Structural Model Index (SMI), trabecular thickness (Tb.Th), trabecular number (Tb.N), trabecular separation (Tb.Sp), and volume Bone Mineral Density (vBMD), were calculated.

To analyse the microstructure of the cancellous bone of the specimen, the metaphysis of the specimen was cut off using a hand-sanded cutter. A Scanning Electron Microscope (SEM, JSM-6490, JEOL, Tokyo, Japan) was used to observe the microstructure of the

samples at room temperature with a working distance of 10 mm – 15 mm under an acceleration voltage of 10 kV. Before observation, the specimens were rinsed with saline to remove blood, mucus, and tissue fluids, dehydrated for 20 min at each concentration (30% to 100%) of alcohol, and then, sprayed with a layer of gold to a 20 nm thickness.

2.4 Landing experiments

In this part, cats with shaved Right Fore (RF) and Right Hind (RH) limbs were trained to land on a plantar pressure measurement platform called MatScan (Texscan Inc.) from an adjustable platform of height between 1 m and 2 m at an increment of 0.2 m (Fig. 1). Additionally, a motion capture system (100 Hz; Vicon Inc.), synchronised to the MatScan, was utilised to collect the spatial positions of reflective markers with a diameter of 9 mm, which were placed over the shoulder blade, shoulder, elbow, wrist joint, and fingertip of the RF limb and the pelvis, hip, knee, ankle joint, and toe of the RH limb. To reduce the measurement artefacts caused by sliding of the markers, the positions of the elbow and knee joints were optimised using MATLAB to be closest to the collected positions of markers using constraints. The detailed description of the constraints adopted for the MATLAB procedure has been reported in our previous study[23].

Based on planar kinematics and inverse dynamics analyses, the kinematic/kinetic data, obtained from the landing experiments, were combined with the segment mass and moment of inertia[24] to calculate the energy absorbed by each joint using MATLAB. In particular, the buffering durations of the forelimbs were defined as the time from the moment the RF paws touched the ground to the moment the RF wrists began to leave the force plate. Meanwhile, the buffering durations of the hindlimbs were defined as the period beginning with the touch-down of the hind paws and ending at the time when the knee flexion reached the maximum.

2.5 Statistical analysis

All data were reported as mean ± Standard Deviation (SD), and one-way analysis of variance (ANOVA) with a post-hoc LSD *t*-test was performed to determine the statistical significance of the test data at a *P* (probability) value of 0.05 (SPSS Inc., Chicago, USA).

3 Results and discussion

3.1 Foot-level buffering mechanism

Representative histological and CT images of the metacarpal pads are presented in Figs. 2a and 2b. The paw pads of cats are composed of an epidermis layer, a dermis layer, and a subcutaneous layer, which are also found in the footpads of human beings, elephants, dogs, and leopards[25–28]. It has recently been proved that there are different microstructure and mechanical properties for each layer, which act as a multistage buffer in dissipating the ground reaction force. For example, the epidermis is identified to have the hardest materials because of the tremendous impact that it is subjected during landing[29]. In contrast, as it performs a major part of energy absorption[28,30], the components of the subcutaneous layer materials are the softest among the three layers. The hardness of the dermis layer is intermediate between those of the epidermis and the subcutaneous layer, just like its spatial position. One study on canine paw pads found that the dermal papilla, a matrix of tissue in the dermis, is inserted in the epidermis[25], creating a honeycomb-like structure which is known to absorb energy when struck[31,32]. From the above discussion, we infer that as a multistage buffer, the layered structure is conducive to buffering the ground forces while maintaining structural integrity.

As the dominant energy absorption site in the pad, the subcutaneous layer was thoroughly investigated. We showed that there are numerous adipose chambers surrounded by collagen fibres that form many closed compartments. We further investigated the amount of elastin and collagen types. The histological images show that elastic fibres are only present in small quantities and are mostly located in the dermis layer. In addition, the distribution of Type I and Type III collagen fibres in the subcutaneous layer is distinctive that collagen fibres surrounding the adipose chambers are mainly collagen I fibres. In contrast, within the chambers, mostly Type III collagen fibres are present. This is because collagen I fibres are composed of thick fibres, being the principal collagen of skin and bone. Therefore, the adipose compartment formed by its surrounding will not be destroyed under the instantaneous higher impact force.

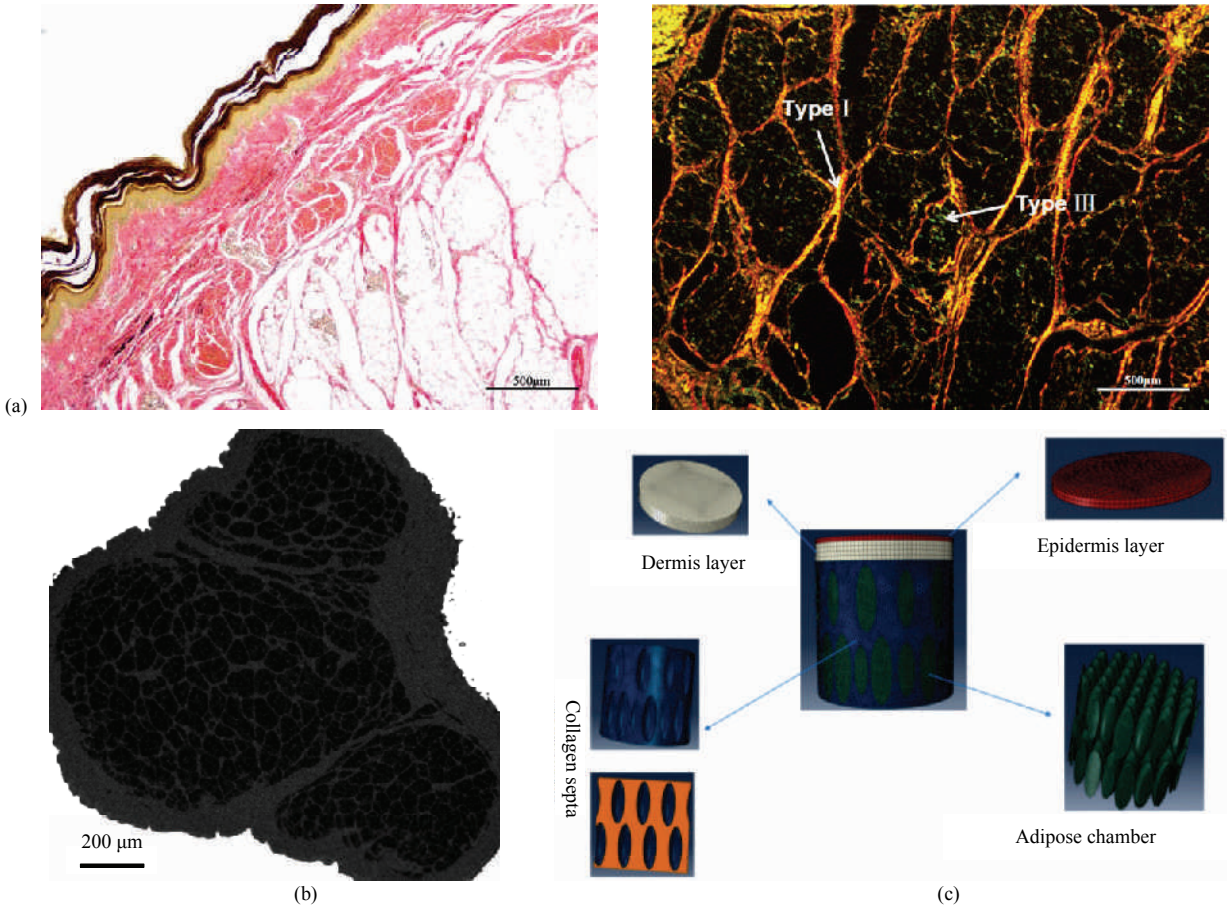

Fig. 2 (a) Representative histological images of the paw pad, stained with Verhoeff-van Gieson stain (left) and Sirius Red stain (right); (b) CT image of the paw pad; (c) FEM composed of the epidermis layer, dermis layer, collagenous membranes, and ellipsoidal adipose chambers.

Type III collagen fibres are always found in more elastic tissues such as blood vessels and skin. They increase the elasticity of fat cells and form visco-elastic properties to cushion the impact more effectively.

However, the 3D microstructure of the adipose compartments has been unknown. Therefore, we performed a micro-CT scanning of the pads and found that the 3D structure of one compartment can be regarded as an ellipsoid even if it was idealised to be a cylinder in previous studies[30] because it has a decreasing cross-sectional area from the middle toward both ends. Combined with the above findings of the layered structure, we established a FEM comprising the epidermis layer, the dermis layer, the collagen septa, and the ellipsoidal adipose chamber, as shown in Fig. 2c. For comparison, another model with cylindrical adipose chambers was established. The stress-strain results (Fig. 3)

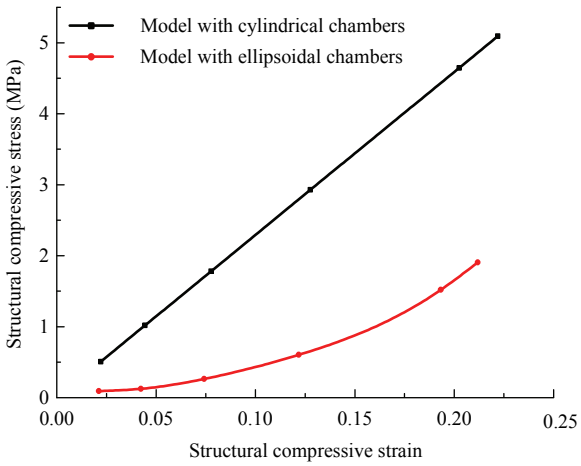

Fig. 3 Stress (Von Mises)-strain curves of the FEMs with cylindrical and ellipsoidal adipose chambers.

show that the two models have similar values of strain, which is basically consistent with the results of

mechanical tests[5]. However, the maximum stress of the cylindrical model is obviously higher, indicating that the ellipsoidal model has greater advantages in buffering the impact force. The trend of the stress-strain curves clearly show that the properties of the ellipsoidal model agree more with the macroscopic nonlinear viscoelastic mechanical properties, suggesting that this model can be used to describe the biomechanical response of the pad under compressive load. Meanwhile, it can be seen from the contour of the Von Mises distributions (Fig. 4) that not only the maximum stress of the cylindrical model is large, but also there is a phenomenon of stress concentration that is not conducive to maintaining the integrity of the structure under impact. In the ellipsoidal model, the stress distribution is relatively uniform, indicating that stress transmission occurs which may be a protective mechanism during impact. In summary, the ellipsoidal adipose chambers in the subcutaneous layer can guide the impact resistance and can provide inspiration for the structural design of relevant impact-resistant materials.

3.2 Limb-level buffering mechanism

During cat landing, it is impossible for paw pads to absorb all the energy, so the limb bones at the limb-level should have a high mechanical strength to resist the impact, ensuring that no fractures occur. As is seen from Table 1, the maximum load, breaking load, stiffness, and elastic modulus of the humeri, femur, and tibia are significantly higher ($P < 0.05$) than those of other bones. This result is expected because the dimensions of the humeri, femur, and tibia are inherently higher than those of other bones. Additionally, no significant differences ($P > 0.05$) are found in mechanical properties between the humeri and femur, however, their mechanical parameters are significantly lower than those of the tibia. Although there are no comparative mechanical data from the bones of other species, it can be seen intuitively that the mechanical strength of cat limb bones is extremely large considering their body size, contributing to resistance in landing injury. At the same time, the hindlimbs exhibit greater mechanical strength due to their femur and tibia compared to the forelimbs.

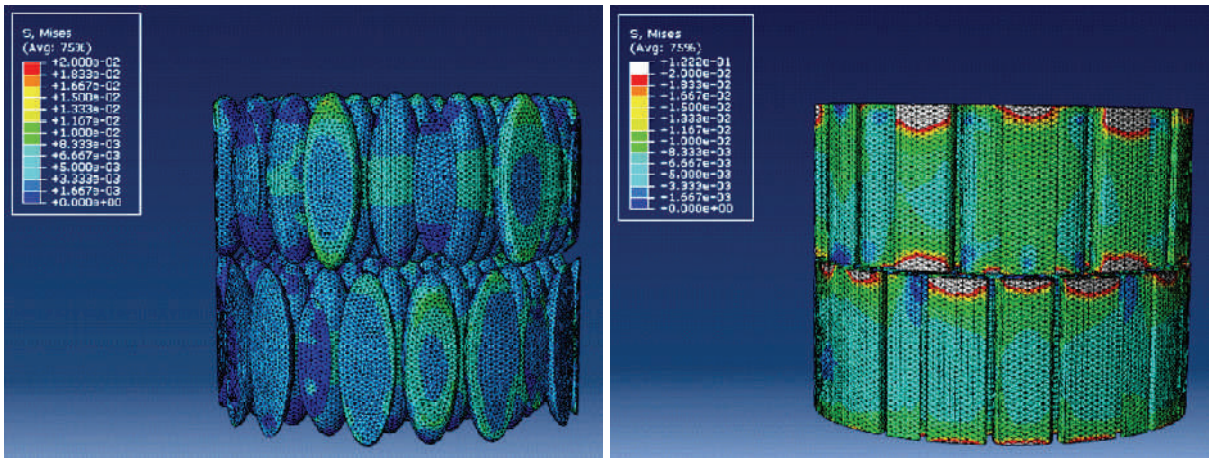

(a) (b)

Fig. 4 Contour of the Von Mises distributions within the ellipsoidal adipose chambers (a) and cylindrical adipose chambers (b).

Table 1 Descriptive data of the three-point bending test*

Measurement (unit)	Humerus[a,b]	Ulna	Radius	Femur[a,b]	Tibia[a]	Fibula
Maximum load (N)	189.04 (20.17)	130.56 (11.83)	100.16 (10.04)	188.25 (19.73)	278.05 (26.10)	17.04 (4.29)
Breaking load (N)	159.28 (13.82)	100.03 (11.41)	91.78 (9.75)	137.06 (12.88)	181.03 (15.23)	9.36 (3.40)
Stiffness ($N \cdot mm^{-1}$)	149.25 (15.96)	110.54 (12.01)	49.42 (7.99)	146.73 (18.07)	316.36 (31.29)	5.07 (1.93)
Elastic modulus (GPa)	12.24 (3.22)	6.76 (2.17)	3.69 (0.84)	12.08 (2.80)	29.47 (4.37)	0.78 (0.11)

* Values in parentheses are the SD; "a" shows statistically significant differences from the ulna, radius and fibula; "b" shows statistically significant differences from the tibia.

The mechanical strength of the bone depends on the microstructure and the composition of the bone tissue[33,34]. Therefore, a comparison of the mechanical properties and microstructure of the limb bones allows better understanding of how cats avoid impact injury to the limbs. The morphometric variables of trabeculae in the limb bones based on the micro-CT images are presented in Table 2. The SMI for the humeri, femur, and tibia is lower than that of other bones ($P < 0.05$), and the BV/TV and Tb.Th of the three bones are relatively higher ($P < 0.05$). With respect to other parameters, there are no significant differences among the six limb bones ($P > 0.05$).

According to the definition of SMI parameter, it is used to represent rod-like or plate-like structures with a value of 0–3 and is independent of the physical dimensions. The closer the value tends to 0, the closer the shape is to a plate-like structure; in contrast, the shape is close to a rod-like structure. In contrast to results of previous studies on how the woodpecker resists head impact injuries[35,36], cat limb bones are found to have more plate-like structures, suggesting that cat limb bones are more impact-resistant. These observations are consistent with the SEM results shown in Fig. 5, in which plate-like trabeculae can be clearly seen.

The SMI value alone is not sufficient to provide accurate information regarding trabecular bone. The Tb.Th, Tb.N, and Tb.Sp of the bone also need to be measured for comparative analysis. These values directly quantify the structure within a three-Dimensional Region of Interest (3-D ROI) and have also been correlated with the ultimate strength of bone[37]. The humeri, femur, and tibia of the cat had more plate-like trabeculae, a greater trabecular thickness, and a higher bone volume fraction. We conclude that the humeri, femur, and tibia of cats exhibit higher mechanical strength and resistance to impact injury as a result of their unique microstructure, including more plate-like trabecular bones, greater thickness, and higher bone volume fraction. These distinctive mechanical properties and microstructure of cat limb bones provide excellent resistance to impact injury during landing. Such information may perhaps inspire the design and optimisation of protective materials for humans.

Table 2 Means and SD of the micro-parameters of the limb bones*

Parameters	Humerus	Ulna	Radius	Femur	Tibia	Fibula
BV/TV (%)	62.37 (1.56)[a]	41.99 (2.45)	47.69 (2.28)	56.92 (1.77)[a]	56.85 (1.62)[a]	45.69 (1.91)
SMI	0.449 (0.17)[a]	1.547 (0.79)	1.845 (0.84)	0.342 (0.09)[a]	0.395 (0.11)[a]	1.653 (0.73)
Tb.Th (μm)	415.96 (19.47)[a]	240.55 (9.28)	253.60 (11.46)	307.44 (15.37)[a]	438.52 (18.20)[a]	269.72 (12.33)
Tb.N (μm^{-1})	0.0014 (0.0003)	0.0018 (0.0004)	0.0011 (0.0002)	0.0019 (0.0003)	0.0013 (0.0002)	0.0017 (0.0002)
Tb.Sp (μm)	243.81 (10.06)	225.69 (11.69)	303.85 (9.98)	229.50 (13.47)	252.82 (11.58)	216.39 (14.63)
vBMD ($g \cdot cm^{-3}$)	0.316 (0.019)	0.289 (0.004)	0.273 (0.007)	0.343 (0.017)	0.310 (0.011)	0.281 (0.008)

* Values in parentheses are the SD; "a" shows statistically significant differences from the ulna, radius and fibula.

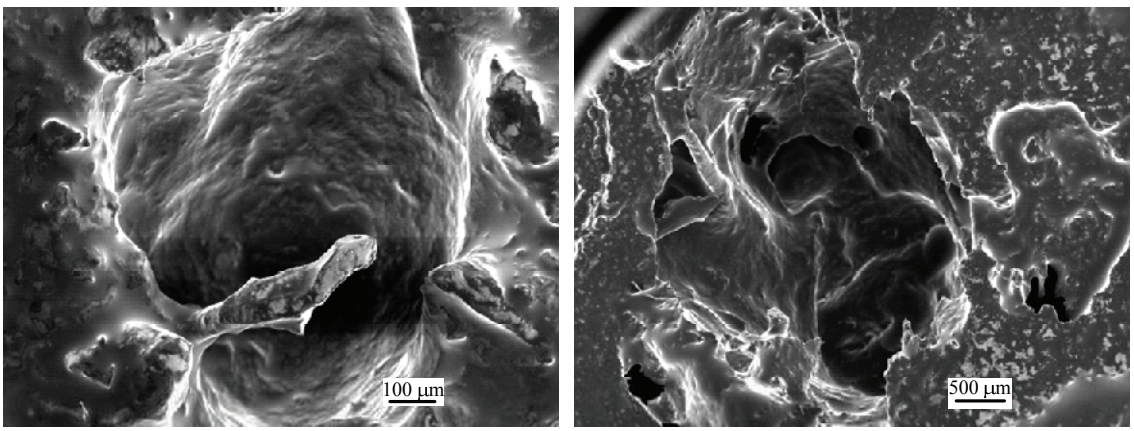

(a) (b)

Fig. 5 SEM images of the proximal femur (a) and tibia (b) of cat.

3.3 Joint-level buffering mechanism

Through coordinated control, energy flow occurs between adjacent joints, so that external and internal forces can be mediated, thus, partial impact energy is absorbed at the joint level. In addition, the advantages of the paw pads and limb bones in buffering are also considered subjectively by the cat for landing strategies. Fig. 6 shows the buffering durations of both limbs for different jump heights. As can be seen, for the six jump heights, the buffering durations of the RF limbs (t_1) are almost the same (approximately 47 ms). By contrast, the buffering durations of the RH limbs (t_2) significantly increase, whereas the time intervals (Δt) decrease with increasing height. The buffering durations of the limbs are related to the Range of Motion (*ROM*) of the corresponding joints. Therefore, the associated joint *ROM*s are shown in Fig. 7. The results show that ROM_1 values significantly decrease, whereas other *ROM* values increase ($P < 0.05$) with jump height, except for ROM_2 values for which no significant differences are observed.

These results show that the forelimbs and hindlimbs attenuate the ground reaction forces mainly by bending joints. At lower heights, the forelimbs are primarily used for buffering, whereas at higher heights, the hindlimbs play a greater role. This is because the hindlimb has greater mechanical strength from the perspective of limb-level and can withstand a larger impact. Interestingly, depending on the jump height, a cat can actively adjust some parameters, such as the initial angle (ROM_1), the buffering durations of the RF limbs (t_1), and the speed of spinal rotation, to ensure that the impact energy is reasonably distributed between the forelimbs and the hindlimbs. This finding is similar to that of a study concerning the energy absorption by the flexible back of a cat, where the muscle stiffness of the cat's back and landing angle can be modulated to absorb the optimal kinetic energy from each landing; this allows the cat's limbs to attenuate the landing impulse more safely and efficiently[38]. This result is also comparable to skipping gaits in human beings, evaluated in a recent study[39], which finds that the subjects actively adjust the parameters of the trailing leg that lands first after the flight phase like the cat's forelimbs and show coupled control with the leading leg like the cat's hindlimbs to

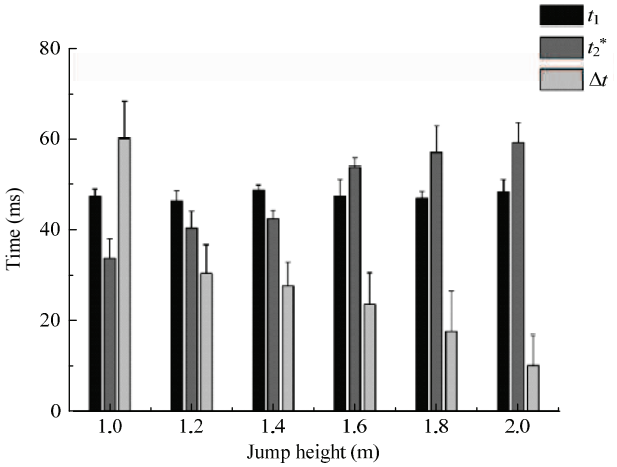

Fig. 6 Means and SD of the buffering durations of the RF (t_1) and RH (t_2) limbs, in time interval (Δt) between the touch-down of the fore paws and the hind paws, for different jump heights. * shows statistically significant differences between jump heights.

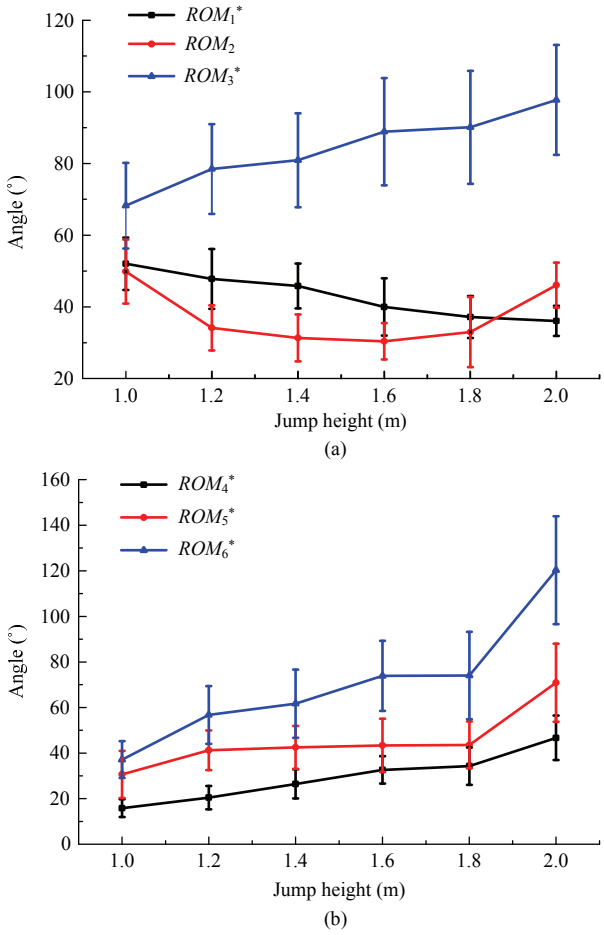

Fig. 7 Mean and SD of the selected *ROM*s versus jumping height. ROM_{1-6} are the ranges of motion of the angle between the fore paw and the ground, wrist joint, elbow joint (a), the angle between the hind paw and the ground, ankle joint and knee joint (b). * shows statistically significant differences between jump heights.

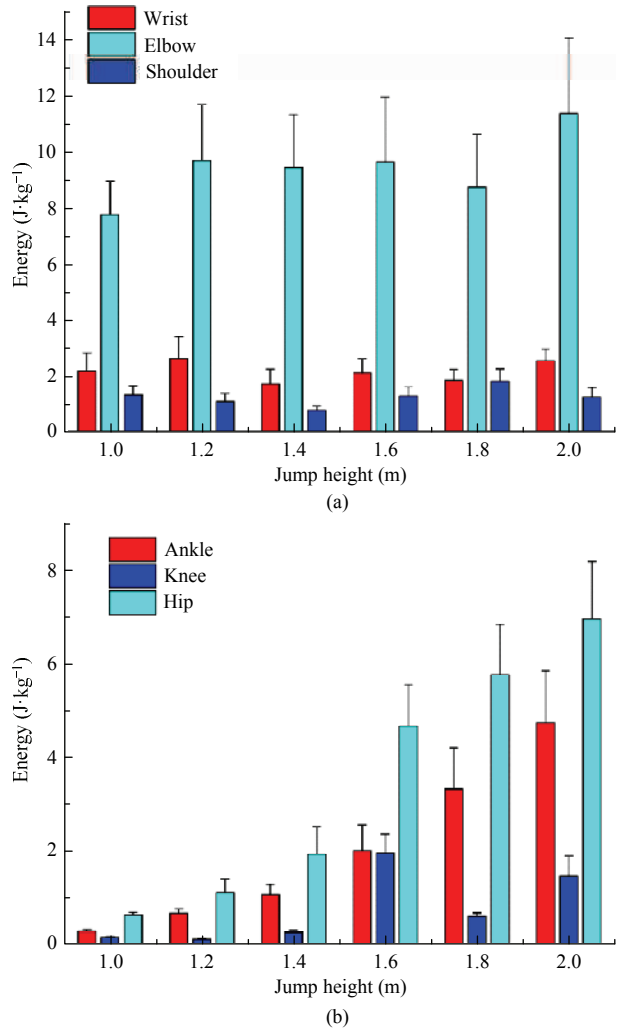

Fig. 8 Mean and SD of joint work for the wrist, elbow, shoulder (a), ankle, knee, and hip (b).

enhance landing stability.

Furthermore, using inverse dynamics, we quantify the contributions of the limb joints to energy absorption (Fig. 8) when landing from different jump heights. Our results show that the elbow and hip are regarded as the primary joints of the forelimbs and hindlimbs, respectively, while absorbing impact energy. We believe this is inseparable to the developed muscle groups around the two joints. Biarticular muscles generate moments at the two joints where the muscles cross to transfer mechanical energy during locomotion[40–42]. The long head of the triceps and biceps with long tendons and muscle fascicules line up in a penniform shape, which is appropriate for dissipating impact energy[43,44]. Similarly, in the hindlimbs, the biceps femoris, semitendinosus, and semimembranosus of cats all have firm tendons and penniform muscle fascicules, allowing absorption of energy by the hip extensors.

4 Conclusion

In this study, the landing process of cats and the biomechanical features of paw pads and limb bones were investigated using biomechanics and biomaterial analysis. Our results show that the microstructure and composition of the paw pads provide the cat with a buffering effect at the foot-level. Notably, the humerus, femur, and tibia exhibit greater mechanical strength and a more impact-resistant trabecular structure, which provides cushioning at the limb-level. Meanwhile, the kinematics of the limb joints and the corresponding muscles are important to absorb impact energy at the joint level. In summary, during cat landing, the paw pads, limb bone materials, and the way joints are controlled in a coordinated manner work together to enable the cat to resist landing injury, and any single factor cannot achieve the function alone. The principle of the multi-level buffering mechanism can provide biological inspiration for reducing human lower limb injuries during landing. The next avenue of future work could be extending the proposed impact-resistant mechanism to exoskeleton design.

Acknowledgment

The work is financially supported by the Defense Industrial Technology Development Program under the Grant JCKY2018601B106 and JCKY2017205B032.

* All supplementary materials are available at https://doi.org/10.1007/s42235-020-0048-x.

References

[1] Vnuk D, Pirkić B, Matičić D, Radišić B, Stejskal M, Babić T, Kreszinger M, Lemo N. Feline high-rise syndrome: 119 cases (1998–2001). *Journal of Feline Medicine & Surgery*, 2004, **6**, 305–312.

[2] Fontanella C G, Carniel E L, Frigo A, Macchi V, Natali A N. Investigation of biomechanical response of Hoffa's fat pad and comparative characterization. *Journal of the Mechanical Behavior of Biomedical Materials*, 2017, **202**, 1–9.

[3] Fontanella C G, Nalesso F, Carniel E L, Natali A N. Biomechanical behavior of plantar fat pad in healthy and

degenerative foot conditions. *Medical & Biological Engineering & Computing*, 2016, **54**, 653–661.

[4] Mihai L A, Alayyash K, Goriely A. Paws, pads and plants: The enhanced elasticity of cell-filled load-bearing structures. *Proceedings of the Royal Society A*: *Mathematical, Physical and Engineering Science*, 2015, **471**, 20150107.

[5] Wu X Q, Pei B Q, Pei Y Y, Hao Y, Zhou K Y, Wang W. Comprehensive biomechanism of impact resistance in the cat's paw pad. *BioMed Research International*, 2019, **2019**, 2183712.

[6] Chi K-J. *Functional Morphology and Biomechanics of Mammalian Footpads*. PhD thesis, ProQuest, Ann Arbor, USA, 2005.

[7] Pei B Q, Wang W, Dunne N, Li X M. Applications of carbon nanotubes in bone tissue regeneration and engineering: SuPeriority, concerns, current advancements, and prospects. *Nanomaterials*, 2019, **9**, 1501.

[8] Li X M, Huang Y, Zheng L S, Liu H F, Niu X F, Huang J, Zhao F, Fan Y B. Effect of substrate stiffness on the functions of rat bone marrow and adipose tissue derived mesenchymal stem cells *in vitro*. *Journal of Biomedical Materials Research Part A*, 2014, **102**, 1092–1101.

[9] Ruimerman R, Huiskes R, Van Lenthe G, Janssen J. A computer-simulation model relating bone-cell metabolism to mechanical adaptation of trabecular architecture. *Computer Methods in Biomechanics and Biomedical Engineering*, 2001, **4**, 433–448.

[10] Wang S H, Yang X, Wang M. The role of body fluid shifts on hindlimb bone loss in tail suspended rats using a novel body fluid alteration device. *Acta Astronautica*, 2019, **159**, 1–7.

[11] Metcalf L M, Dall'Ara E, Paggiosi M A. Validation of calcaneus trabecular microstructure measurements by HR-pQCT. *Bone*, 2018, **106**, 69–77.

[12] Best A, Holt B, Troy K, Joseph H. Trabecular bone in the calcaneus of runners. *PLoS ONE*, 2017, **12**, e0188200.

[13] Tsegai Z J, Skinner M M, Gee A H. Trabecular and cortical bone structure of the talus and distal tibia in Pan and Homo. *American Journal of Physical Anthropology*, 2017, **163**, 784–805.

[14] Meachen-Samuels J A, Blaire V V, Allen F A. Radiographs reveal exceptional forelimb strength in the sabertooth cat, smilodon fatalis. *PLOS ONE*, 2010, **5**, e11412-.

[15] Farrell B J, Bulgakova M A, Sirota M G. Accurate stepping on a narrow path: Mechanics, EMG and motor cortex activity in the cat. *Journal of Neurophysiology*, 2015, **114**, 2682–2702.

[16] Brown N P, Bertocci G E, Cheffer K A. A three dimensional multiplane kinematic model for bilateral hind limb gait analysis in cats. *PLOS ONE*, 2018, **13**, e0197837.

[17] Kane T R, Scher M P. A dynamical explanation of the falling cat phenomenon. *International Journal of Solids & Structures*, 1969, **5**, 663–666.

[18] Zhang Z Q, Yu H, Yang J L, Wang L L, Yang L M. How cat lands: Insights into contribution of the forelimbs and hindlimbs to attenuating impact force. *Chinese Science Bulletin*, 2014, **59**, 3325–3332.

[19] Mckinley P A, Smith J L. Visual and vestibular contributions to prelanding EMG during jump-downs in cats. *Experimental Brain Research*, 1983, **52**, 439–448.

[20] Leyva-Mendivil M F, Page A, Bressloff N W, Limbert G. A mechanistic insight into the mechanical role of the stratum corneum during stretching and compression of the skin. *Journal of the Mechanical Behavior of Biomedical Materials*, 2015, **49**, 197–219.

[21] Sims A M, Stait-Gardner T, Fong L, Morley J W, Price W S, Hoffman M, Simmons A, Schindhelm K. Elastic and viscoelastic properties of porcine subdermal fat using MRI and inverse FEA. *Biomechanics & Modeling in Mechanobiology*, 2010, **9**, 703–711.

[22] Sun L W, Fan Y B, Li D Y, Zhao F, Xie T, Yang X, Gu Z T. Evaluation of the mechanical properties of rat bone under simulated microgravity using nanoindentation. *Acta Biomaterialia*, 2009, **5**, 3506–3511.

[23] Wu X Q, Pei B Q, Pei Y Y, Wu N, Zhou K Y, Hao Y, Wang W. Contributions of limb joints to energy absorption during landing in cats. *Applied Bionics and Biomechanics*, 2019, **2019**, 3815612.

[24] Hoy M G, Zernicke R F. Modulation of limb dynamics in the swing phase of locomotion. *Journal of Biomechanics*, 1985, **18**, 49–60.

[25] Miao H B, Fu J, Qian Z H, Ren L Q, Ren L. How does paw pad of canine attenuate ground impacts? A multi-layer cushion system. *Biology Open*, 2017, **6**, 1889–1896.

[26] Qian Z H, Ren L, Ren L Q. A coupling analysis of the biomechanical functions of human foot complex during locomotion. *Journal of Bionic Engineering*, 2010, **7**, S150–S157.

[27] Hubbard C, Naples V, Ross E, Carlon B. Comparative analysis of paw pad structure in the clouded leopard (*Neofelis nebulosa*) and domestic cat (*Felis catus*). *Anatomical Record*, 2010, **292**, 1213–1228.

[28] Weissengruber G, Egger G, Hutchinson J, Groenewald H B, Elsässer L, Famini D, Forstenpointner G. The structure of the cushions in the feet of African elephants (*Loxodonta*

africana). *Journal of Anatomy*, 2006, **209**, 781–792.

[29] Meyer W, Bartels T, Tsukise A, Neurand K. Histochemical aspects of stratum corneum function in the feline foot pad. *Archives of Dermatological Research*, 1990, **281**, 541–543

[30] Ker R F. The design of soft collagenous load-bearing tissues. *Journal of Experimental Biology*, 1999, **202**, 3315–3324.

[31] Yamashita M, Gotoh M. Impact behavior of honeycomb structures with various cell specifications-numerical simulation and experiment. *International Journal of Impact Engineering*, 2005, **32**, 618–630.

[32] Burlayenko V, Sadowski T. Effective elastic properties of foam-filled honeycomb cores of sandwich panels. *Composite Structures*, 2010, **92**, 2890–2900.

[33] Ciarelli M, Goldstein S, Kuhn J, Cody D, Brown M. Evaluation of orthogonal mechanical properties and density of human trabecular bone from the major metaphyseal regions with materials testing and computed tomography. *Journal of Orthopaedic Research*, 1991, **9**, 674–682.

[34] Dalén N, Hellström L-G, Jacobson B. Bone mineral content and mechanical strength of the femoral neck. *Acta Orthopaedica Scandinavica*, 1976, **47**, 503–508.

[35] Wang L Z, Zhang H Q, Fan Y B. Comparative study of the mechanical properties, micro-structure, and composition of the cranial and beak bones of the great spotted woodpecker and the lark bird. *Science China Life Sciences*, 2011, **54**, 1036–1041.

[36] Wang L Z, Niu X F, Ni Y K, Xu P, Liu X Y, Lu S, Zhang M, Fan Y B. Effect of microstructure of spongy bone in different parts of woodpecker's skull on resistance to impact injury. *Journal of Nanomaterials*, 2013, **2013**, 924564.

[37] Perilli E, Baleani M, Öhman C, Baruffaldi F, Viceconti M. Structural parameters and mechanical strength of cancellous bone in the femoral head in osteoarthritis do not depend on age. *Bone*, 2007, **41**, 760–768.

[38] Zhang Z Q, Yang J L, Yu H. Effect of flexible back on Energy absorption during landing in cats: A biomechanical investigation. *Journal of Bionic Engineering*, 2014, **11**, 506–516.

[39] Müller R, Andrada E. Skipping on uneven ground: Trailing leg adjustments simplify control and enhance robustness. *Royal Society Open Science*, 2018, **5**, 172114.

[40] Miller S, Van Der Burg J, Van Der Meche F. Coordination of movements of the hindlimbs and forelimbs in different forms of locomotion in normal and decerebrate cats. *Brain Research*, 1975, **91**, 217–237.

[41] Betts B, Smith J L, Edgerton R, Collatos T C. Telemetered EMG of fast and slow muscles in cats. *Brain research*, 1976, **117**, 529–533.

[42] McKinley P, Smith J, Gregor R. Responses of elbow extensors to landing forces during jump downs in cats. *Experimental Brain Research*, 1983, **49**, 218–228.

[43] English A W. An electromyographic analysis of forelimb muscles during overground stepping in the cat. *Journal of Experimental Biology*, 1978, **76**, 105–122.

[44] Konow N, Azizi E, Roberts T J. Muscle power attenuation by tendon during energy dissipation. *Proceedings of the Royal Society B*: *Biological Sciences*, 2011, **279**, 1108–1113.